The Electronic Structure of Crystalline $Li_{21}Si_5$. A Cluster Approach to a γ-Brass Structure

Rafael Ramírez*, Reinhard Nesper, and Hans Georg von Schnering
Max-Planck-Institut für Festkörperforschung, Stuttgart

Michael C. Böhm
Institut für Physikalische Chemie, Physikalische Chemie III,
Technische Hochschule Darmstadt

Z. Naturforsch. **41 a**, 1267–1282 (1986); received July 14, 1986

The electronic structure of crystalline $Li_{21}Si_5$ is investigated by semiempirical MO (molecular orbital) calculations of the INDO (intermediate neglect of differential overlap) type in the framework of a finite cluster approach. The complex solid-state ensemble with 416 atoms per unit cell is divided into 16 cluster units M_{26} that form the three-dimensional structure. These M_{26} clusters have two different chemical compositions and act as formal donor and acceptor fragments, namely $D = (Li_{20}Si_6)$ and $A = (Li_{22}Si_4)$, having the formal net charges $q(D) = -4$ and $q(A) = +4$. The electronic structures of these finite building units are rationalized by the semiempirical MO model. The one-electron energies of $(Li_{20}Si_6)^{4-}$ and $(Li_{22}Si_4)^{4+}$ are derived on the basis of fragment interactions between the site sets (tetrahedral, octahedral, cube-octahedral) that build up the different M_{26} units. The canonical MO's are transformed by means of the Edmiston-Ruedenberg localization procedure in order to come to a clear representation of the chemical bond in the two clusters. In $(Li_{20}Si_6)^{4-}$ a coincidence of the classical valence rules and the existence of nonclassical many-center bonds is found. $(Li_{22}Si_4)^{4+}$ on the other side violates the counting schemes because of an excess of 2 electrons (electron octets at Si). The model calculations show however that the octet rule is strictly fulfilled in the Si subspace. The Li centers allow for the formation of an additional bonding cage orbital due to in-phase interactions between the Li 2s AO's. This MO is occupied by the two excess electrons which are left after filling the valence orbitals associated to Si. The formation of such a one-electron level is not considered in classical models. The Li-Si interaction in $Li_{21}Si_5$ is of covalent nature and is comparable to the metal-nonmetal bonds in other lithium silicides. The Li-Li contacts are nonbonding in the framework of the Hartree-Fock approximation. The observed solid-state structure of the binary phase can be explained by intercluster interactions between the different donor and acceptor fragments.

1. Introduction

Compounds of the IA and IIA with the IIIB to VIB maingroup elements have been the subject of considerable activities over the past decades due to their interesting chemical and physical properties [1–3]. These compounds are usually called Zintl-phases in order to appreciate the pioneering work of E. Zintl in that field of intermetallic compounds [4]. The structures show a broad spectrum of one-, two- and three-dimensional networks as well as isolated cluster arrangements. The electronic structures of such phases are interpreted in terms of formal electron counting schemes which are known as Zintl-Klemm and Mooser-Pearson rules [5–8]. These topological approaches have been developed several years ago and allow for empirical correlations between stoichiometry, solid-state structure and physical properties. Nowadays the electronic structures of simpler Zintl-phases with small repeat-units have been investigated in the framework of sophisticated solid-state approaches based on APW (augmented plane wave), OPW (orthogonalized plane wave) or local density functional schemes [9–14]. Unfortunately, the prohibitive computational expenditure restricts these approaches to a narrow class of compounds, thereby leaving a large theoretical deficit in the case of phases with complex composition and/or extended unit cell dimensions.

In recent contributions [15, 16, 17] we have studied the electronic structures of complex binary

* Present address: Institut für Physikalische Chemie, Physikalische Chemie III, Technische Hochschule Darmstadt.

Reprint requests to Prof. Dr. H. G. von Schnering, Max-Planck-Institut für Festkörperforschung, Heisenbergstr. 1, D-7000 Stuttgart 80, West Germany.

0340-4811 / 86 / 1100-1267 $ 01.30/0. – Please order a reprint rather than making your own copy.

and ternary phases containing Si, Li and Mg, respectively, by means of an improved INDO (intermediate neglect of differential overlap) crystal orbital (CO) approach [18, 19]. These computational tight-binding studies lead to a consistent picture of the nature of the chemical bond and allowed for a reliable reproduction of several experimental observables, e.g. geometry, band gap and charge distribution. The unit cell dimensions of the employed lithium silicides were far beyond the computational capacities of classical solid-state approaches. In our theoretical studies [15–17] we tried furthermore to find bridging relations between empirical counting schemes and quantitative values from numerical band structure calculations. Thereby we verified also the electronic origin responsible for the limitations of the well-known counting rules.

The present contribution extends our studies of the electronic structures of lithium silicides to the cubic phase $Li_{21}Si_5$ crystallizing with 416 atoms per unit cell. In contrast to our recent investigations, where the translation symmetry of the lattice had been taken into account explicitly, we had to restrict this analysis to a cluster approach, i.e. the electronic structure of the three-dimensional (3D) ensemble is interpreted on the basis of finite building blocks forming the solid-state arrangement. This numerical limitation is caused by the complex 3D structure of $Li_{21}Si_5$ which prevents any vindicated reduction of the spatial symmetry. The bonding capabilities of suitable subunits of the binary lithium silicide are studied by the afore mentioned improved INDO Hamiltonian [19] which has been designed to reproduce the computational results of ab initio MO (molecular orbital) schemes of higher accuracy.

Earlier experimental investigations in the Li rich part of the Li/Si binary system lead to the compound $Li_{22}Si_5$ [20]. A detailed reinvestigation of this phase, however, has shown that the correct composition is $Li_{21}Si_5$ [21]. The structure is related to that of the γ-brasses and therefore a theoretical investigation of $Li_{21}Si_5$ seems to be of some interest. The phase violates the empirical counting rules for semiconductors. In order to complete the valence shell of the five Si atoms per formula unit, 20 electrons are formally required from the Li atoms. If this picture is accepted, an excess of one Li atom per formula unit is present in $Li_{21}Si_5$. Alternatively it is possible to classify $Li_{21}Si_5$ according to the valence electron concentration (VEC) approach of Hume-Rothery [22, 23]. In this counting scheme, originally developed for transition metals, a VEC = 20.5/13 is derived for $Li_{21}Si_5$. This value is close to 21/13 which is the VEC of the γ-brasses. This close analogy, which is also found in the crystal structures (see below) suggests to interpret $Li_{21}Si_5$ as a main-group counterpart of Hume-Rothery γ-phases.

The organization of the present article is as follows. The crystal structure of $Li_{21}Si_5$ is described in the next section. The cluster units employed in this investigation are presented in Chapter 3. Section 4 gives a summary of the computational details. The electronic structure of the different clusters is explained in the paragraphs 5 and 6. Comparisons will be made with findings of quantum chemical calculations of lithiated hydrocarbons [24–28] and small molecules containing Si skeletons [29]. Special emphasis will be given to the validity of the octet rule in hyperlithiated molecules [30]. The three-dimensional arrangement of the clusters and their mutual stabilization in the solid state is the subject of paragraph 7.

2. The $Li_{21}Si_5$ Structure

$Li_{21}Si_5$ crystallizes in the space group $F\bar{4}3m$ (T_d^2, no. 216) with a lattice parameter $a = 18.71$ Å and 416 atoms per unit cell ($Z = 16$). The unit cell contains 16 cluster M_{26} formed by $4 + 4 + 6 + 12$ atoms which belong to an inner tetrahedron (IT), an outer tetrahedron (OT), an octahedron (OH) and an cube-octahedron (CO), respectively. The general topological arrangement of the M_{26} clusters is shown in Figs. 1 and 2. The point symmetry of the subunits $M_{26} = (IT + OT + OH + CO)$ is $\bar{4}3m - T_d$.

In order to show the similarities between the structures of $Li_{21}Si_5$ and of γ-brass we have displayed the group-subgroup symmetry relations in Figure 3. This type of correlation leads to a transparent representation of the complex structure and can be used to rationalize modifications of bonding capabilities in solid-state ensembles as response to structural changes. The close connection between symmetry group-subgroup relations and altered physical or chemical properties has been substantiated by Bärnighausen in a large number of examples [31].

Two symmetry reductions are necessary to connect the structure of the aristotype Cu_5Zn_8 with

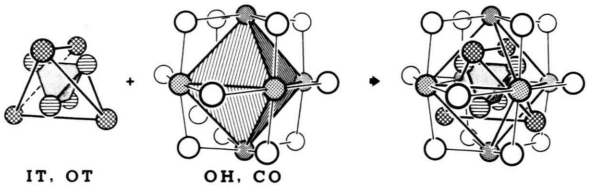

Fig. 1. The four site sets IT, OT, OH and CO, respectively, that built the M_{26} cluster units of $Li_{21}Si_5$. *Left:* Combination of the two tetrahedra IT and OT. *Middle:* Combination of the octahedron OH (dotted circle) and the cube-octahedron CO. *Right:* Complete M_{26} arrangement.

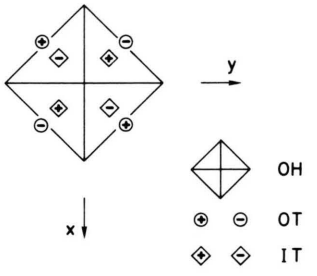

Fig. 2. Schematic representation of the two tetrahedral (IT, OT) and the octahedral (OH) site sets of the M_{26} units.

that of $Li_{21}Si_5$. In the first step the body-centered lattice is transferred into a primitive one due to a klassengleiche transformation (k 2) ($I\bar{4}3m \rightarrow P\bar{4}3m$). The point group of the crystal is thereby conserved but one half of the translational symmetry operations is lost. This operation is accompanied by a doubling (from 1 to 2) of the number of topological inequivalent clusters. In the second step ($P\bar{4}3m \rightarrow F\bar{4}3m$) the k 2 transformation is combined with a doubling of the lattice parameter. The number of inequivalent building units is consequently enlarged from 2 to 4 (see Fig. 3).

The M_{26} clusters of the $Li_{21}Si_5$ structure have two different compositions, namely $A = Li_{22}Si_4$ and $D = Li_{20}Si_6$. Moreover, both types exhibit two topologically slightly different units, namely A, A′ and D, D′, respectively. The distribution of the Li and Si atoms on the four site sets IT, OT, OH and CO in the fragments A, A′, D and D′ is summarized in Table 1. The IT and CO sets are occupied by lithium atoms. With respect to OT and OH, the combination OT(Si) + OH(Li) is realized in the cluster $Li_{22}Si_4$ and the combination OT(Li) + OH(Si) in the cluster $Li_{20}Si_6$.

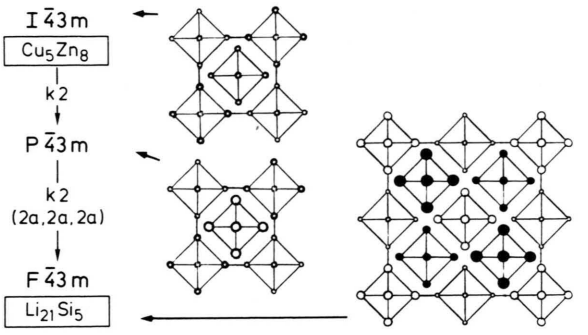

Fig. 3. Symmetry group-subgroup relation between Cu_5Zn_8 (γ-brass) and $Li_{21}Si_5$. This correlation shows the reduction of the I lattice of γ-brass to the F lattice of $Li_{21}Si_5$. *Left:* Symmetry relations between the two structures. *Right:* The different numbers of symmetry-inequivalent units.

Table 1. Atomic occupation of the site sets IT, OT, OH and CO, respectively, in the four cluster species A, A′, D and D′ forming the binary Zintl-phase $Li_{21}Si_5$.

Site set	A, A′ = $Li_{22}Si_4$	D, D′ = $Li_{20}Si_6$
IT	4 Li	4 Li
OT	4 Si	4 Li
OH	6 Li	6 Si
CO	12 Li	12 Li

Table 2. Important intracluster distances (Å) in the four clusters M_{26} A, A′, D and D′ of $Li_{21}Si_5$. The indices in parenthesis symbolize the four possible site sets IT, OT, OH and CO, respectively.

Atom 1 – Atom 2	$Li_{22}Si_4$		Atom 1 – Atom 2	$Li_{20}Si_6$	
	A	A′		D	D′
Li(IT) – Li(IT)	2.74	3.92	Li(IT) – Li(IT)	3.08	3.51
Si(OT) – Si(OT)	4.78	4.36	Li(OT) – Li(OT)	4.44	4.29
Li(OH) – Li(OH)	4.68	4.64	Si(OH) – Si(OH)	4.71	4.79
Li(CO) – Li(CO)	3.92	4.31	Li(CO) – Li(CO)	3.50	3.86
Si(OT) – Li(IT)	2.85	2.93	Si(OH) – Li(IT)	2.72	2.77
Si(OT) – Li(OH)	2.89	2.79	Si(OH) – Li(OT)	2.83	2.85
Si(OT) – Li(CO)	2.65	2.63	Si(OH) – Li(CO)	2.95	2.99
Li(IT) – Li(OH)	2.71	2.73	Li(IT) – Li(OT)	2.75	2.78
Li(IT) – Li(CO)	2.95	2.73	Li(IT) – Li(CO)	2.63	2.83
Li(OH) – Li(CO)	3.01	3.06	Li(OT) – Li(CO)	2.72	2.40

Important interatomic separations within the four subunits A, A′, D and D′ are collected in Table 2. Details of the crystal structure have been reported elsewhere [21]. Therefore only a short summary of the essential results is given in this context. The Li – Si bond lengths are found in an interval

Table 3. Relative positional parameters of the M_{26} clusters in γ-brass (Cu_5Zn_8) [34] and in $Li_{21}Si_5$. The largest deviations between both phases have been printed in bold face. The listed parameters (x, t) are relative to the cluster centers given in parenthesis. The last line contains the z values of CO.

Cluster	Cu_5Zn_8 (0 0 0)		A (0 0 0)		A′ ($\frac{1}{4}\frac{1}{4}\frac{1}{4}$)		D ($\frac{3}{4}\frac{3}{4}\frac{3}{4}$)		D′ ($\frac{1}{2}\frac{1}{2}\frac{1}{2}$)	
Atomic site	M	$\frac{x}{2}, \frac{z}{2}$	M	x, z	M	x, z	M	x, z	M	x, z
IT 4 ($x\,x\,x$)	Zn	0.055	Li	0.052	Li	**0.074**	Li	0.058	Li	**− 0.066**
OT 4 ($x\,x\,x$)	Cu	− 0.086	Si	− 0.090	Si	− 0.082	Li	− 0.084	Li	**0.081**
OH 6 ($x\,0\,0$)	Cu	0.178	Li	0.177	Li	0.175	Si	0.178	Si	0.181
CO 12 ($x\,x\,z$)	Zn	0.156	Li	0.159	Li	0.163	Li	0.154	Li	0.158
		0.018		0.012		0.001		0.022		0.012

between 2.65 to 2.99 Å, values that are typical for lithium silicides [16, 17, 32, 33]. The shortest Li−Li contacts observed in the two cluster types are in the range of nonbonding Li−Li pairs in Li-containing Zintl-phases. The separations between the Si atoms are too large to allow for any direct interactions.

Table 3 gives a comparison of the positional parameters of the four site sets (IT, OT, OH, CO) in $Li_{21}Si_5$ and the aristotype Cu_5Zn_8. Some details in the two structures differ substantially. The inner tetrahedron is strongly enlarged in the A′ unit. This leads to Li(IT)−Li(IT) separations of ca. 3.9 Å which exceed the Li−Li contacts in A (2.7 Å) by ca. 1.2 Å. The inner and outer tetrahedra of D′ are exchanged in comparison to their orientation in A, A′ and D, respectively. The atoms of IT occupy the sites ($\bar{x}, \bar{x}, \bar{x}$) in D′, but ($x, x, x$) in the other three clusters. This is equivalent to a 90° rotation of D′ relative to the orientation of A, A′ and D in the unit cell. Empirical rules how to distribute the available atomic species among different cluster types have been derived by Pearson and co-workers [35] in the case of γ-brass phases. On the basis of geometrical criteria they were able to show that the atoms of the minority component N in alloys $M_{21}N_5$ (M, N any components with N of larger size larger than M) occupy the position OH, OH, OT, OT in the direction of the space diagonals of the cubic unit cell. It is one of the aims of the present study to explain such preferences in the framework of electronic structure theories. For this purpose it is necessary to analyze the bonding capabilities of the four cluster subunits, to develop simple schemes for their coupling and to compare the theoretical predictions with experimental observations.

3. Topologically Different Clusters A, A′ ($Li_{22}Si_4$) and D, D′ ($Li_{20}Si_6$) as Building Units of $Li_{21}Si_5$

The M_{26} cluster units A, A′, D and D′ are used for the interpretation of the electronic structure of $Li_{21}Si_5$. To generate physically meaningful electron distributions for the units $Li_{22}Si_4$ and $Li_{20}Si_6$, we make use of one restrictive assumption: only "closed shell" configurations are considered. The one-particle levels are either doubly occupied or empty. It will become clear that this model simulates the "preparation" of unperturbed electron donor and acceptor components forming the 3 D structure. In lowest order of approximation the four clusters are treated as isolated systems. Their mutual coupling is of course accompanied by a partial charge transfer from the "donor" to the "acceptor" moieties. The direction and strength of the transfer will be monitored by simple test calculations. In order to come to a clear picture of the nature of the inter-cluster coupling the electronic structures of the isolated building blocks will be discussed with special emphasis to their abilities to interact with adjacent cluster units. Of course the suggested model approach (i.e. fragmentation of the whole 3 D structure into finite building blocks with formal donor and acceptor functions) is a simplified theoretical description which has been adopted to facilitate the analysis of the solid-state electronic structure of $Li_{21}Si_5$.

Semiempirical SCF (self-consistent-field) calculations of the INDO type have been performed for the $Li_{20}Si_6$ and $Li_{22}Si_4$ units with different one-electron populations and total charges $(Li_{20}Si_6)^0$, $(Li_{20}Si_6)^{2-}$, $(Li_{20}Si_6)^{4-}$; $(Li_{22}Si_4)^0$, $(Li_{22}Si_4)^{2+}$ and

$(Li_{22}Si_4)^{4+}$. The iterative procedures converged into stable "closed shell" configurations with one-electron wave functions transforming according to the irreducible representations of the point group $\bar{4}3\,m-T_d$ *only* in the case of $(Li_{20}Si_6)^{4-} = D/D'$ and $(Li_{22}Si_4)^{4+} = A/A'$. In this context we have to mention explicitly that no stable mean-field solution was feasible for $(Li_{22}Si_4)^0$.

$(Li_{20}Si_6)^{4-}$ fulfills obviously the octet rule, i.e., the valence orbitals of the six electronegative Si atoms are completely filled in a cluster containing 48 valence electrons. In the 34 electron system $(Li_{22}Si_4)^{4+}$ the octet configuration for Si is already reached in the case of 32 valence electrons. This pretended deviation between the actual filling scheme and the classical octet rule will be discussed in some detail in Section 6.

The three-dimensional arrangement found in $Li_{21}Si_5$ will be rationalized on the basis of intercluster interactions between $(Li_{22}Si_4)^{4+}$ and $(Li_{20}Si_6)^{4-}$. Although the nature of this interaction transmitted via Li–Si contacts [9, 15, 17] is mainly covalent, charge transfer between both cluster types has to be expected. $(Li_{20}Si_6)^{4-}$ is of course the formal "donor" unit and $(Li_{22}Si_4)^{4+}$ the "acceptor".

4. Computational Details

The semiempirical INDO MO approach employed for the present analysis has been described in [19]. In contrast to the original parametrization of the electron-core attraction we have neglected penetration effects in the MO calculations of the binary lithium silicide. The recently developed approximations used for calculation of the electron-core interaction are nonvalid in electronic systems with highly coordinated main-group atoms [36]. The used integral evaluation is therefore reduced to the standard scheme of semiempirical ZDO (zero differential overlap) variants [37].

For each of the finite Li_mSi_n clusters several occupation patterns have been iterated up to SCF convergence. The HF (Hartree-Fock) filling schemes have been selected on the basis of one-electron calculations of the Wolfsberg-Helmholtz type. The computational results summarized in the subsequent sections correspond in any case to the solutions of lowest energy. As an additional restriction we have requested that the orbital wave functions transform according to the irreducible representations of the point group $\bar{4}3\,m-T_d$. The iterative cycles have been controlled by an accelerated Hartree damping of the bond-order matrices [38]. An energy criterion of 10^{-4} a.u. has been accepted to terminate the SCF calculations. The charge distributions are determined by a Mulliken population analysis [39]. The strength of covalent diatomic interactions has been measured by the widely used Wiberg bond indices [40].

In order to simplify the analysis of the MO data we adopt local coordinate systems for the atomic sites. The local z-axes in each tetrahedron and octahedron point away from the corresponding cluster centers (exo orientation). The x-axes of the octahedral site sets coincide with the internuclear vectors within OT. The local y-axes are analogously oriented with respect to the inner tetrahedra. The structural parameters of [21] have been used to define the cluster geometry.

5. The Electronic Structure of $(Li_{20}Si_6)^{4-}$

The topology of the cluster units D and D′ is roughly comparable. Therefore it can be expected that their electronic structures are also very similar. In order to come to a clear representation of the bonding interactions in $(Li_{20}Si_6)^{4-}$ we start from the six electronically isolated Si atoms and analyze their coupling with the Li sites IT and OT, respectively (first step), as well as of CO (second step).

The membership of the Si (3s, $3p_x$, $3p_y$, $3p_z$) and Li (2s, $2p_x$, $2p_y$, $2p_z$) AO's to the irreducible representations of the point group $\bar{4}3\,m$ is summarized in Table 4. The six 3s functions in the Si OH cage split into symmetry adapted linear combinations transforming according to $a_1 + e + t_2$; the

Table 4. Distribution of symmetry adapted linear combinations of the atomic orbitals (s, p_x, p_y and p_z) of the site sets OH and OT to the irreducible representations Γ_i of the point group $\bar{4}3\,m$. The local coordinate system as defined in the text has been used.

Γ_i	AO's at OH	AO's at OT
a_1	s, p_z	s, p_z
e	s, p_z	$(p_x + p_y)$
t_2	s, p_z, $(p_x + p_y)$	s, p_z, $(p_x + p_y)$
t_1	$(p_x + p_y)$	$(p_x + p_y)$

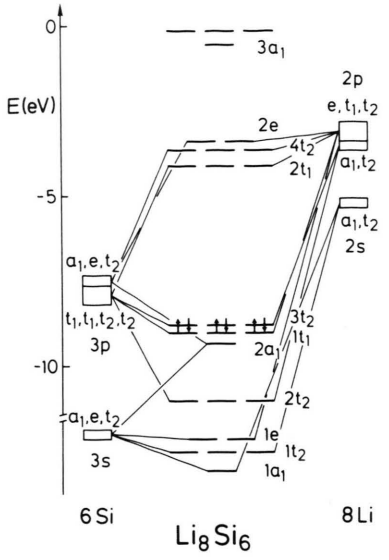

Fig. 4. Schematic representation of the molecular orbitals of the central Li_8Si_6 fragment of the "donor" clusters D, D′ = $(Li_{20}Si_6)^{4|-}$. The MO's are classified according to the irreducible representations of the point group $\bar{4}3$ m. The highest filled orbital ($3t_2$) is labeled by arrows.

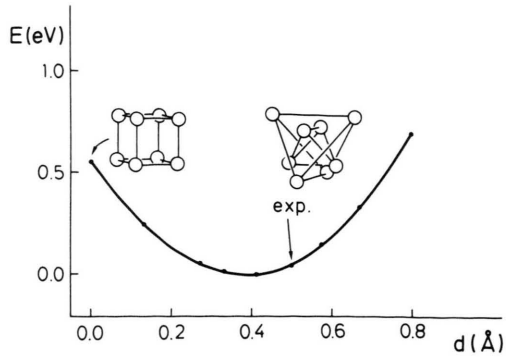

Fig. 5. Energy profile for the structural transition of the eight central Li atoms from a cube-like arrangement with equivalent metal sites to a geometry consisting of two coupled tetrahedrons of different spatial sizes. The geometric coordinate d measures the difference between the radii associated to spheres that circumscribe the spatial extension of the two site sets IT and OT. The cube-like arrangement corresponds thus to $d = 0$. The energy has been given in relative units. The experimentally observed geometry has been labeled in the potential energy curve.

same irreducible representations are of course valid for the six (local) Si $3p_z$ functions. The remaining 12 AO's of the Si site set ($3p_x$ and $3p_y$) can be combined to cluster states of $t_1 + t_1 + t_2 + t_2$ symmetry. The Li 2s and $2p_z$ AO's of IT and OT split into $a_1 + t_2$ representations. The $2p_x$ and $2p_y$ functions can be combined to fragment orbitals, transforming according to $t_2 + t_1 + e$.

A semiquantitative MO diagram of the subunit Li_8Si_8 is displayed in Figure 4. The following canonical MO scheme is derived for the inner sphere of $(Li_{20}Si_6)^{4-}$. Six low-lying MO's ($1a_1$, $1t_2$, $1e$) are significantly separated from the remaining filled valence orbitals. The corresponding wave functions are prevailingly of Si 3s character and are stabilized mainly by Li 2s admixtures. Only one occupied fragment MO derived from the Si $3p_z$ AO's is predicted in the subunit Li_8Si_6 ($2a_1$). A slight hybridization between the two totally symmetric linear combinations leads to nonvanishing Si $3p_z$ amplitudes in $1a_1$ and to Si 3s admixtures in $2a_1$. The latter combination is thereby efficiently hybridized away from the Si cage (exo direction). The remaining Si $3p_z$ linear combinations belong to the virtual MO space. With respect to the Si $3p_x$ and $3p_y$ functions the strongest stabilization due to Li–Si coupling is derived for the $2t_2$ combination which contains in-phase Li 2s admixtures from the OT site set. The $3t_2$ and $1t_1$ MO's are the two highest occupied levels of the subunit Li_8Si_6. The lobes of the corresponding Si orbitals are partially directed towards adjacent Si centers of OH; the interaction with the surrounding Li surface is thereby reduced. The last member of Si $3p_x$ and $3p_y$ ($2t_1$) is the lowest unfilled orbital of the employed subfragment. Inspection of Fig. 4 shows that the aforementioned lowest empty MO's of the subunit Li_8Si_6 ($2t_1$, $4t_2$, $2e$) are energetically separated by several eV from the remaining unoccupied functions which are largely localized at the Li centers.

We have modified the size of the central Li cages IT and OT, respectively, in order to find the electronic origin favouring the observed arrangement of two coupled tetrahedra of different spatial extensions in comparison to a possible cube-like geometry containing eight equivalent Li sites. In Fig. 5 we have shown the energy profile for this structural transition. The geometric coordinate d in this display is the difference between the two distances of the two tetrahedral site sets IT and OT from their common center. The cubic-like arrangement is consequently characterized by $d = 0$. The size of the cube has been averaged on the basis of the experimental geometry of the two Li tetrahedra.

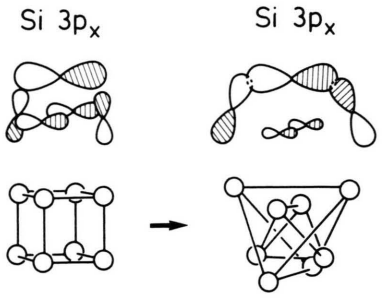

Fig. 6. Simplified representation of the Li–Si interaction stabilizing the $1t_1$ orbital of the Li_6Si_8 fragment of the $(Li_{20}Si_6)^{4-}$ cluster. *Left:* Overlap between the $3p_x$ AO of Si and suitable Li functions in the case of a cube-like Li arrangement. *Right:* Li–Si overlap for the experimentally verified tetrahedral geometry (IT and OT). The metal-nonmetal overlap is optimized in the latter case. The Si position relative to the Li arrangement is displayed in the Figs. 1 and 7, respectively.

Table 5. Localization (in percent) of the filled valence orbitals and the lowest empty states of the cluster $D = (Li_{20}Si_6)^{4-}$. The total Li contributions have been divided into contributions from the three different site sets IT, OT and CO, respectively. The highest occupied MO (HOMO) has been labeled by an asterisk.

MO	Type	Si(OH)	Li(IT)	Li(OT)	Li(CO)	$\sum$ Li
$5t_2$	Li	33	1	0	66	67
$3a_1$	Li	8	3	2	87	92
2e*	Si (p_z)	85	6	4	5	15
$4t_2$	Si (p_z)	68	5	4	23	32
$2t_1$	Si (p_x, p_y)	67	1	5	27	33
$1t_1$	Si (p_x, p_y)	65	3	7	25	35
$2a_1$	Si (p_z, s)	68	9	5	18	32
$3t_2$	Si (p_x, p_y)	64	1	4	31	36
$2t_2$	Si (p_x, p_y)	45	8	9	38	55
1e	Si (s), Li	62	6	9	23	38
$1t_2$	Si (s), Li	47	15	12	26	53
$1a_1$	Si (s), Li	32	19	16	32	68

The observed structure (i.e. combination of two tetrahedra of different sizes) is reproduced with remarkable accuracy. The experimental parameter d amounts to ca. 0.5 Å while the model calculations lead to a value of $d \approx 0.4$ Å. The energy difference between the two minima is ca. 0.05 eV (≈ 5 kJ/mol).

The Li–Si interaction favouring the observed IT/OT arrangement is schematized in Figure 6. The tetrahedral coordination allows for a more efficient stabilization of the $1t_1$ cluster orbital. This is symbolized in the diagram on the righthand side which shows the enhanced overlap between the $3p_x$ AO's of Si and suitable Li orbitals as a function of the distortion from the cube-like arrangement into the direction of two tetrahedra. The remaining cluster states are only insignificantly influenced by this deformation.

The one-electron levels symbolized in in Fig. 4 are roughly conserved if the central Li_8Si_6 fragment is saturated by the Li atoms of the CO site set leading to the final $(Li_{20}Si_6)^{4-}$ donor. The conservation of the MO sequence predicted for Li_8Si_6 in $Li_{20}Si_6$ is caused by the fact that the Li amplitudes of the CO unit differ (with one exception) not strongly in the various cluster orbitals. The localization properties of all occupied orbitals as well as the lowest empty MO's of $(Li_{20}Si_6)^{4-}$ are summarized in Table 5. It can be seen that the Si admixtures dominate in the filled Fermi-sea; the corresponding amplitudes are predicted within an interval of 32% ($1a_1$, minimum) to 85% (2e, HOMO). Table 5 shows furthermore that the Li admixtures from CO exceed usually the net metal contributions from the two tetrahedral site sets. This is only in part a size effect (i.e. 12 Li atoms belonging to the CO site set vs. 4 Li atoms IT and OT, respectively). The main reason leading to this difference is a topological one. The Li atoms of CO have two Si contacts in the employed cluster unit while the metal sites belonging either to IT or OT are coordinated to three Si sites. This bridging function of Li is also found in other crystalline lithium silicides [15–17] and in simpler molecular species [29].

To render possible a more transparent interpretation of the nature of the Li–Si interactions in $(Li_{20}Si_6)^{4-}$ we transformed the canonical MO wave functions into a set of localized orbitals by means of the intrinsic Edmiston-Ruedenberg localization procedure [41]. Important results for the localized orbitals are summarized in Table 6. The unitary

Table 6. Localization (in percent) of the localized orbitals of the cluster $D = (Li_{20}Si_6)^{4-}$. The contributions from the Si octahedron as well as the three Li site sets are given.

Leading Si contribution	Number of localized orbitals	Si	Li(IT)	Li(OT)	Li(CO)
Si 3 s	6	53.3	9.6	10.2	26.9
Si 3 p_x	6	58.7	1.4	12.8	27.1
Si 3 p_y	6	53.8	5.5	3.1	37.6
Si 3 p_z	6	76.1	9.4	3.9	10.6

transformation leads to six one-electron wave functions with 53.3% Si 3s character and vanishing 3p amplitudes. The associated Li–Si interactions are of a nonclassical multi-center type and span four adjacent Li centers of IT and OT, respectively, as well as the four nearest Li CO atoms. A schematic display of such a two-electron-nine-center bond is shown in Figure 7. Six linear combinations associated to the Si $3p_x$ AO's and six localized MO's with Si $3p_y$ character are derived by the unitary transformation. The relative Si and Li contributions of these functions are roughly comparable with the localization properties of the Si "3s orbitals". In a simplified picture both MO sets can be interpreted as seven-center bonds formed by two Li atoms from the IT or OT site sets and four nearest neighboring Li atoms from the CO cage. One example of this multi-center bond is shown in Figure 7. The last set of six transformed MO's is formed by Si $3p_z$-type orbitals which are strongly localized at the Si centers (76%). This explains immediately that canonical Si $3p_z$ descendants in Li_8Si_6 or $(Li_{20}Si_6)^{4-}$ are found at higher energies in comparison to $3p_x/3p_y$ linear combinations. The Si "$3p_z$" functions are stabilized due to a Li surface formed by 8 atomic sites (four from the IT and OT site sets, four from the CO site set). A simplified representation of the shape of this local function is also given in Figure 7.

The transformation of the delocalized MO's of $(Li_{20}Si_6)^{4-}$ into a local representation shows two interesting features of the studied cluster.

a) The results summarized in Table 6 indicate that s/p hybridization at Si is without larger significance, the 3s and 3p levels of the nonmetal atoms form two energetically separated domains of one-electron wave functions. An exception is the aforementioned hybridization between $1a_1$ and $2a_1$. The absence of s/p hybridization is consistent with LCAO calculations of simple main-group molecules that have shown that the s/p intermixing is a peculiarity of the atomic species of the first row [42].

b) The schematic display in Fig. 7 shows a rather unusual coincidence between the general validity of the $(8-N)$ rule and the occurrence of nonclassical multi-center bonds that cover up to nine atomic sites (1 Si, 8 Li) of the employed cluster. In simple finite Fermion systems the validity of a $(8-N)$ law is conventionally coupled to the degree of freedom

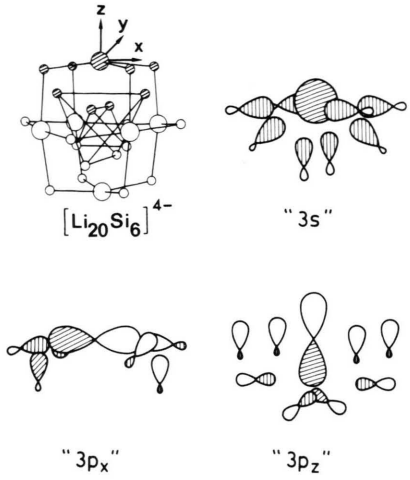

Fig. 7. Simplified representation of the localized occupied orbitals of the $(Li_{20}Si_6)^{4-}$ cluster. *Top left:* The local coordinate system and the topology of this unit are shown in the left side. The hatched areas indicate those atoms that are included in the 3 schematic representations. *Top right:* Function formed by a Si 3 s AO. Six such combinations are observed. *Bottom left:* Orbital of Si $3p_x$ character. The six Si $3p_y$ are similar to the $3p_x$ set and are thus not included in the display. *Bottom right:* Example of the six "lone-pair" functions. The largest AO contributions are due to the Si $3p_z$ AO set which are stabilized by a surface of eight adjacent metal centers.

Table 7. Atomic net charges q_A and q'_A of $(Li_{20}Si_6)^{4-}$. The net charges q'_A correspond to the cluster $(Li_{20}Si_6)^{4-}$ surrounded by a set of 14 Li atoms which simulate intercluster interaction in the 3 D solid.

Atom	Site set	q_A	q'_A
Si	OH	− 0.86	− 0.55
Li	IT	0.24	0.26
Li	OT	0.15	0.15
Li	CO	− 0.03	− 0.06

to represent chemical bonds in terms of two-electron-two-center combinations [43]. This "classical" conformity of localizability and the validity of the $(8-N)$ rule is no longer valid in complex cluster structures where the coordination numbers are larger than in molecular species.

In Table 7 we have summarized the atomic net charges in the $(Li_{20}Si_6)^{4-}$ cluster; Wiberg bond indices are collected in Table 8. Large excess charges are predicted at the electronegative Si atoms, i.e., the donor strength of D/D′ in the first place will be determined by the central Si skeleton. The Li atoms of the inner tetrahedra show the

Atomic pair	W_{AB}
Si–Li(IT)	0.27
Si–Li(OT)	0.31
Si–Li(CO)	0.54
Li(IT)–Li(IT)	0.03
Li(IT)–Li(OT)	0.05
Li(IT)–Li(CO)	0.06
Li(OT)–Li(CO)	0.09
Li(OT)–Li(OT)	0.01
Li(CO)–Li(CO)	0.10

Table 8.
Wiberg bond indices W_{AB} for selected atomic pairs of the intracluster-type in $(Li_{20}Si_6)^{4-}$.

largest charge deficit followed by the Li sites of OT. A small surplus (− 0.03) of electronic charge is predicted for the metal atoms of the surrounding CO site set. Therefore donor properties associated with this Li cage at the CO positions must be expected.

The Li–Si bond indices are found in an interval between 0.27 (metal atoms of IT) and 0.54 (metal atoms of CO). The bond indices to the Li sites of the outer tetrahedra exceed by 15% the corresponding elements with respect to the inner tetrahedra. The electronic origin for this difference has been discussed in connection with the Figs. 5 and 6.

The Li–Si bond indices are characteristic for diatomic Li–Si interactions that are largely covalent in nature [16, 17]. In Li–C bonds it is still a controversial question whether the nature of this interaction is mainly covalent or ionic [24–28, 44, 45]; the reduced electronegativity of Si (relative to C) together with the more diffuse Si AO wave functions enhance however covalent interactions in lithium silicides. The Li–Li indices in $(Li_{20}Si_6)^{4-}$ are small in comparison to the Li–Si elements and are typical for nonbonding Li–Li contacts.

To derive a semiquantitative measure for the strength and direction of the donor capabilities of $(Li_{20}Si_6)^{4-}$ we have performed model calculations where this unit is surrounded by a surface of 14 Li atoms which simulate intercluster interactions. The adopted Li arrangement corresponds to the intercluster geometry realized in $Li_{21}Si_5$. Six of the external Li sites are located into the exo directions with respect to the OH(Si) cage. Always four "layer" atoms are coordinated to the IT and OT sites sets. By means of this model (i.e. $(Li_{20}Si_6)$ plus (Li_{14})) cluster charges of $(Li_{20}Si_6)^{-2.35}$ and $(Li_{14})^{+2.35}$ are calculated, i.e. 1.65 electrons have been transferred from the formal "donor" unit to the surrounding "acceptor" surface. In the second column of Table 7 we have sumarized the atomic net charges of the donor unit in the field of the 14 surrounding Li centers. It is also clear why the expected donor-type Li atoms of CO do not participate in charge transfer processes. The intercluster interaction is prevailingly determined by Li–Si contacts, a diatomic coupling which exceeds the Si–Si and Li–Li pairs. The employed model contains only an outer surface of Li functions. Therefore only interactions of the type Li(external)–Si(OH) are approximated in this approach. On the other side, a larger charge transfer from the Si atoms is predicted by the simplified model; the charge excess is reduced from − 0.86 to − 0.55. On the basis of these results it can be suggested that the leading channels of the charge transfer are associated to the external metal ("acceptor") atoms that are coordinated to the site sets OH and OT respectively. The magnitude of the transfer in these directions exceed the interaction with IT centers by ca. 80%. The quantum chemical origin for this preferential transfer channel can be extracted from Table 5. The frontier orbitals 2e and $4t_2$ as well as the $2a_1$ linear combination form strongly Si-centered cluster orbitals with $3p_z$ AO amplitudes that point to the external Li atoms coordinated to the OH site sets. The following occupied MO ($2t_1$) has mainly Si $3p_x$ character (42% Si $3p_x$, 25% Si $3p_y$). These $3p_x$ AO's point to the external Li centers that are coordinated to the OT site set.

The population of the four AO's of Si is in line with the aforementioned donor properties. The largest charge is found within the $3p_z$ function (1.53e); 1.17e are calculated for $3p_z$, 1.07e for $3p_y$ and 1.09 for the 3s orbital.

6. The Electronic Structure of $(Li_{22}Si_4)^{4+}$

The analysis of the electron structure of the acceptor unit $(Li_{22}Si_4)^{4+}$ will be divided into two steps. In the first one the interaction of the Li sites of IT and OH with the Si atoms forming the outer tetrahedron is investigated; in the second step the changes of the one-electron properties due to the surrounding Li surface formed by the outer cube-octahedron are taken into account.

A simplified MO diagram of the central $Li_{10}Si_4$ subunit is displayed in Figure 8; we have adopted the geometry of A. The orbital energies of A′ are

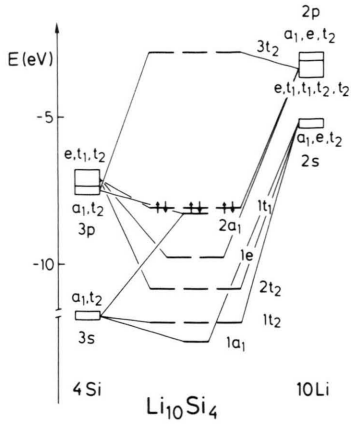

Fig. 8. Schematic representation of the molecular orbitals of the central $(Li_{10}Si_4)$ fragment of the "acceptor" cluster $(Li_{20}Si_4)^{4+}$. The MO's are classified according to the irreducible representations of the point group $\bar{4}3$ m. The highest filled orbital $(1\,t_1)$ is labeled by arrows.

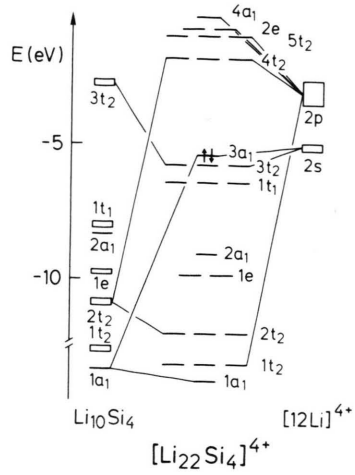

Fig. 9. Schematic representation of the molecular orbitals of the $(Li_{22}Si_4)^{4+}$ acceptor cluster (A). The cluster orbitals are constructed by means of the one-electron states derived for $Li_{10}Si_4$ (schematized on the left side, see Fig. 8) and symmetry adapted linear combinations associated to the surrounding Li cube-octaheadron $[(12\,Li)^{4+}]$ (right side). The MO's are classified according to the irreducible representations of the point group $\bar{4}3$ m. The higest filled orbital $(3\,a_1)$ is labeled by arrows. The one-electron energies of the charged cluster are given in relative units.

similar to the one-electron levels of A. The four lowest filled orbitals of the subunit $Li_{10}Si_4$ ($1a_1$ and $1t_2$) are of predominant Si 3s character, stabilized by 2s admixtures of the two Li site sets. All one-electron functions associated to Si $3p_x$ and $3p_y$ are occupied in the selected central unit. They show in-phase interactions with Li states hybridized into the direction of the outer Si tetrahedra. This Li–Si coupling is maximized in the $2t_2$ MO; strong bonding interactions are caused by the metal sites of OH. The remaining one-particle functions belonging to this set are 1e and $1t_1$, respectively. The $2a_1$ level is the only occupied function associated to the Si $3p_z$ AO set. The remaining Si $3p_z$ functions are unoccupied. They form the lowest empty MO of the $Li_{10}Si_4$ moiety ($3t_2$).

The one-particle energies of the complete $(Li_{22}Si_4)^{4+}$ cluster are schematized in Fig. 9 (cluster A). A comparison with Fig. 8 shows the occupancy of the $3t_2$ (Si $3p_z$ linear combination) MO in the M_{26} unit. In analogy to $(Li_{20}Si_6)^{4-}$ this has its origin in the surronding surface due to the 12 Li atoms from the CO site set. The relative energetic separation of most of the remaining one-electron states is roughly conserved in the full acceptor unit. In addition to the sixteen occupied MO's, which are descendants of the valence AO's of the non-metal centers, a new linear combination ($3a_1$) is predicted in the filled MO space which has no counterpart in the $(Li_{20}Si_6)^{4-}$ "donor". The character of this MO differs strongly from the one-electron properties listed in Table 5. This is demonstrated in Table 9 where we have summarized the localization properties of the highest filled and lowest unfilled MO's of A and A′. The $3a_1$ level is an exception in the filled Fermi-sea as the metal contributions to the MO wave function exceed 80%. The orbital is an in-phase combination of Li 2s AO's, in the first place from atomic sites of the OH and CO site sets. Small antibonding Li–Si interactions in $3a_1$ are overcompensated due to the in-phase overlap between the Li centers. The localization properties of the remaining occupied MO's, on the other hand, are roughly comparable to the numerical results derived for $(Li_{20}Si_6)^{4-}$.

The acceptor strength of A and A′ is determined by the shape of the lowest empty orbitals in the two types of positively charged clusters. The $4t_2$ LUMO of A contains 42% Si amplitudes ($3p_x/3p_y$). The nonmental contributions are enhanced up to 52% in the A′ cluster at the cost of the metal admixtures from the CO site set. The next acceptor levels $5t_2$, 2e and $4a_1$ are of predominant Li character, the leading AO contributions come from the OH and CO site sets. These symmetry species are descen-

Table 9. Localization (in percent) of the filled valence orbitals and the lowest empty one-particle functions of the two $(Li_{22}Si_4)^{4+}$ acceptor clusters A and A′. The total contributions have been devided into that of the three different site sets IT, OH and CO, respectively. The highest filled MO's (HOMO) of both units (A/A′) have been labeled by an asterisk.

MO	Type	Si(OT)	Li(IT)	Li(OH)	Li(CO)	Li
		Cluster A				
$4a_1$	Li	3	6	23	68	97
2 e	Li	31	0	31	38	69
$5t_2$	Li	13	2	40	45	87
$4t_2$	Li, Si (p_x, p_y)	42	4	10	44	58
$3a_1$*	Li	18	11	16	55	82
$3t_2$	Si (p_z)	77	9	2	12	23
$1t_1$	Si (p_x,p_y)	72	4	14	10	28
$2a_1$	Si (p_z, s)	75	7	2	16	25
1 e	Li, Si (p_x, p_y)	49	11	13	27	51
$2t_2$	Li, Si (p_x, p_y)	42	8	20	30	58
$1t_2$	Li, Si (s)	48	17	15	20	52
$1a_1$	Li, Si(s)	31	21	21	27	69
		Cluster A′				
$4a_1$	Li	10	18	19	53	90
2 e	Li	31	0	30	39	69
$5t_2$	Li	8	6	37	49	92
$4t_2$	Si (p_x, p_y), Li	52	9	8	31	48
$3t_2$*	Si (p_z)	68	9	4	19	32
$3a_1$	Li	22	18	12	48	78
$1t_1$	Si (p_x, p_y)	72	7	13	8	28
$2a_1$	Si (p_z, s)	71	6	4	19	29
1 e	Li, Si (p_x, p_y)	48	15	13	24	52
$2t_2$	Li, Si (p_x, p_y)	43	9	20	28	57
$1t_2$	Li, Si (s)	48	14	16	22	52
$1a_1$	Li, Si (s)	34	19	21	26	66

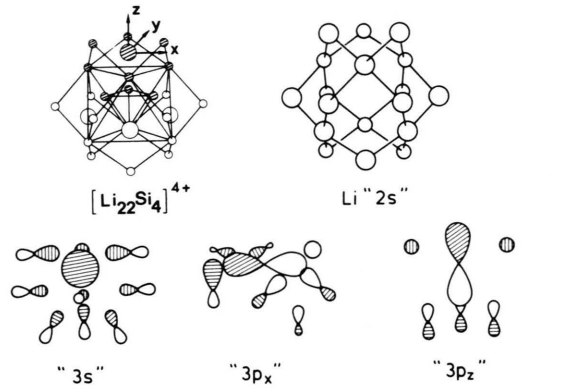

Fig. 10. Simplified representation of the occupied orbitals of the $(Li_{22}Si_4)^{4+}$ cluster (geometry A) after the application of the Edmiston-Ruedenberg localization procedure. The coordinate system and the topology of this unit are shown on the top left. The z axis coincides with the direction of the threefold symmetry axis. The hatched areas identify those atoms that are included in the 3 schematic representations (lower half). On the bottom left an example for a Si 3 s MO is shown. The localized Si 3 p_x/3 p_y linear combination is schematized in the bottom middle. The bottom right display corresponds to a Si 3 p_z "lone-pair" function strongly localized of the nonmetal center(s). On the top right we have shown the Li 2 s cage orbital allowing for the stabilization of an additional occupied MO which is not associated to the Si atoms. This state is delocalized over all Li sites of the $(Li_{22}Si_4)^{4+}$ cluster. The number of transformed orbitals and the localization properties are discussed in the text.

Table 10. Localization (in percent) of the one-electron wave functions after the application of the Edmiston-Ruedenberg localization procedure to $(Li_{22}Si_4)^{4+}$.

Leading AO contribution	Number of localized orbitals	Si	Li(IT)	Li(OH)	Li(CO)
Si 3 s	4	55.1	13.0	12.6	19.3
Si 3 p_x/p_y	8	49.9	8.6	17.2	24.3
Si 3 p_z	4	76.9	10.5	0.3	12.3
Li 2 s cage orbital	1	1.1	11.9	22.1	64.9

dants of the six 2 p_z AO's localized at the OH Li site sets.

In analogy to the donor cluster we applied also in this case (here A cluster) the Edmiston-Ruedenberg localization procedure to come to a clear representation of the electronic interactions in $(Li_{22}Si_4)^{4+}$. The numerical results of the unitary transformation are collected in Table 10. Typical nonmetal linear combinations are found in 16 localized MO's that split into three groups formed by Si 3s, 3 p_x/3 p_y and 3 p_z AO's. The functions are again many-center bonds (Table 6). Schematic displays of these localized orbitals are shown in Figure 10. Four MO's with large Si (3s) amplitudes are predicted by the theoretical approach (Fig. 10, left). The nonmetal AO is stabilized by suitable orbitals from the three nearest Li sites of IT, OH and CO, respectively. The net interaction thus can be described as two-electron-ten-center coupling. Eight localized MO's are predicted that are descendants of the Si 3 p_x and 3 p_y AO sets. The Si AO's are coupled to seven neighboring metal centers. Three Li sites belong to the CO site set, three atoms are provided from OH and one from IT. In a simplified picture this interaction is a two-electron-eight-center bond (Fig. 10, middle). A schematic representation of the Si 3 p_z functions of the acceptor shows that the MO wave function is extended over one Si site and six Li atoms (Fig. 10, right).

The last localized MO of Table 10 is a pure Li 2s combination which is derived from the $3a_1$ cage orbital. This function remains delocalized over all Li centers in spite of the application of the localization procedure; the Si admixtures are negligibly small.

The existence of such a MO wave function is a solid-state counterpart of occupied linear combinations in smaller hyperlithiated molecules such as $(CLi_4)^{2-}$, $(CLi_5)^{1-}$ and $(CLi_6)^0$ (molecules with 10 valence electrons) [27, 28, 30, 46]. The electronic stabilization of such linear combinations has been explained recently by Reed and Weinhold [30]. In the first step MO's are formed where the nonmetal centers (Si) have completed their octet configuration. If this center (these centers) is (are) surrounded by a cage of metal atoms additional electrons can be filled into a bonding linear combination provided by the 2s levels of the cage atoms. The charge dependence of this interaction via possible modifications of the electronegativity of Li will be analyzed in a subsequent contribution [47]. The vanishing Si contributions of the cage orbitals show explicitly that the "octet" rule is not violated in the 34-electron clusters. The corresponding MO is exclusively restricted to the cage formed by the Li site sets (Figure 10). It is thus clear why the classical valence rules (Zintl-Klemm, Mooser-Pearson) fail in this binary phase. In these schemes the electrons are completely associated to the electronegative atoms while the formation of a cage orbital formed by the electropositive subspace is not taken into account. It is an important property of $Li_{21}Si_5$ that the $(8-N)$ rule is valid as long as only the Si subspace is considered. Here we find a 1:1 correspondence between the validity of classical rules and the existence of nonclassical multi-center bonds. This coincidence is lost with the cage orbital as the electropositive centers are not considered in the classical counting rules. The necessary condition for the stabilization of such a cage function is the existence of atomic species with diffuse AO wave functions in order to allow for an efficient overlap between the atomic sites.

The atomic net charges q_A of the two clusters A and A′ are displayed in Table 11 while the Wiberg bond indices are summarized in Table 12. The Li sites with acceptor character (OH and CO) show the largest charge deficit. The surplus of electronic charge of Si is slightly smaller than in the donor fragment. The individual AO population of Si is now 1.12e, 1.01e, 1.01e and 1.54e for the Si 3s, $3p_x$, $3p_y$ and $3p_z$ functions. With respect to Si $3p_x$ and $3p_y$ we have predicted acceptor properties. The analysis shows that they have the lowest electron densities. The Si $3p_z$ population in the acceptors is comparable with the number derived for the $(Li_{20}Si_4)^{4-}$ donor. The magnitude of the Wiberg indices for bonding Li–Si contacts is close to the corresponding W_{AB} elements of $(Li_{20}Si_6)^{4-}$.

Table 11. Atomic net charges q_A and q'_A of A, A′ = $(Li_{22}Si_4)^{4+}$. The charges q'_A correspond to the cluster A = $(Li_{22}Si_4)^{4+}$ surrounded by a layer of six Li_3Si groups which simulate intercluster interactions with respect to the OH site set of the acceptor fragment.

Atom	Site set	q_A (A)	q'_A (A)	q_A (A′)
Li	IT	0.12	0.25	0.05
Si	OT	− 0.67	− 0.77	− 0.59
Li	OH	0.26	0.07	0.26
Li	CO	0.39	0.12	0.38

Table 12. Wiberg bond indices W_{AB} for selected intracluster pairs of $(Li_{22}Si_4)^{4+}$.

Atomic pair	W_{AB} (A)	W_{AB} (A′)
Si–Li(IT)	0.28	0.29
Si–Li(OH)	0.31	0.30
Si–Li(CO)	0.40	0.39
Li(IT)–Li(IT)	0.05	0.03
Li(IT)–Li(OH)	0.07	0.08
Li(IT)–Li(CO)	0.08	0.10
Li(OH)–Li(CO)	0.09	0.08
Li(OH)–Li(OH)	0.02	0.02
Li(CO)–Li(CO)	0.07	0.07

A simplified model for the intercluster interaction with respect to $(Li_{22}Si_4)^{4+}$ is simulated by an external layer of six (Li_3Si)-groups that are coordinated to the Li atoms of the OH and CO site sets. This allows for a reproduction of the coupling Si(exter.)–Li(OH + CO). In the second row of Table 11 we have summarized the modification of the atomic net charges due to this interaction. The Li atoms of OH and CO show the largest increase of electronic charge. This is in line with the discussed acceptor properties of $(Li_{22}Si_4)^{4+}$.

7. The Three-Dimensional Arrangement of the Different Cluster Units in the Binary Phase

A schematic representation of the three-dimensional cluster arrangement is shown in Figure 11. For

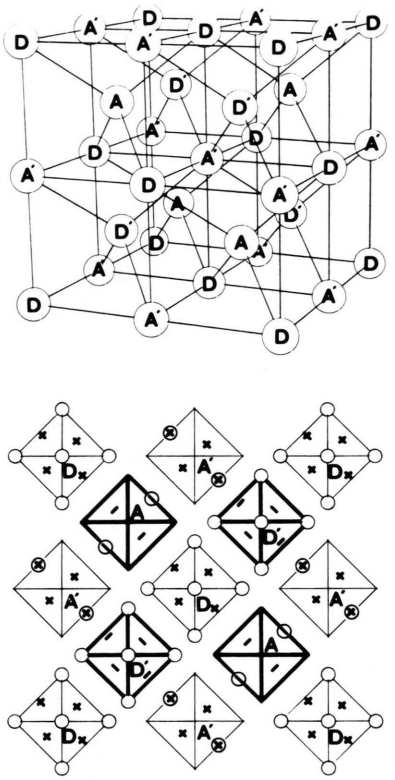

Fig. 11. *Top:* Simplified representation of the three-dimensional arrangement of the four cluster species A, A', D and D' in the cubic cell of $Li_{21}Si_5$. Only the cluster centers are indicated. *Bottom:* Projection of the unit cell along the z direction. In the diagram we have only considered the atoms of the site sets IT, OT and OH of the cluster. Octahedra are symbolized by thin lines (centered at $z = 0$) and thick lines (centered at $z = 1/4$); this representation schematizes the OH frames. The atomic positions of the site sets OT and IT are labeled by + and − symbols according to their height relative to the corresponding cluster centers. Only the positions allowing for intercluster interactions are included in the display. The IT positions are of course those closer to the cluster-centers. The Si positions are indicated by circles.

the moment it is only important to rationalize the spatial arrangement of the cluster units.

The electronic factors that determine the 3D arrangement of A, A', D and D' can be rationalized by means of the donor-acceptor properties discussed in the last sections. The intercluster interaction is exclusively determined by Li−Si bonds. The Si−Si contacts via atomic centers fulfilling the octet rule do not lead to a stabilization of the 3D solid as the interaction between the Si electrons is strongly antibonding [48]. Also the nonbonding Li−Li pairs do not participate in intercluster coupling. Table 13 contains the atomic centers and the relevant AO's that contribute to the different intercluster interactions; the possible combinations of donor (D, D') and acceptor (A, A') pairs leading to intercluster interactions are also included in the table.

a) *Interaction-type I* is caused by the OH site sets of both donor and acceptor units. The remarkable donor properties of $(Li_{20}Si_6)^{4-}$ by means of Si $3p_z$ combinations into the exo direction of the OH site sets and the corresponding acceptor properties of $(Li_{22}Si_4)^{4-}$ caused by the metal $2p_z$ orbitals of OH allow for a strong intercluster bonding. This leads to a mutual coupling that forms a NaCl structure arrangement between donor and acceptor units (Figure 12). The Si atoms occupy the site sets OH, OT, OH for the series donor/acceptor/donor into the direction of the space diagonal of the cubic unit cell.

$Li_{21}Si_5$ contains two acceptor units (A, A') and two donors (D, D'), a building principle that causes the formation of two interpenetrating NaCl substructures shifted by (1/4, 1/4, 1/4) relative to each other. The Si atoms of $Li_{21}Si_5$ occupy therefore the site sets OH OH OT OT in this direction. In Sect. 2

Table 13. Important intercluster interactions that lend to the 3D structure of $Li_{21}Si_5$. Three coupling patterns, namely type I, type II and type III are derived on the basis of the model calculations. The table contains the atomic centers contributing to the coupling, the associated site sets and the relevant AO's. In the last row the cluster moieties (i.e., A, A', D and D') are collected that participate in the coupling mechanism.

Interaction type	Donor $(Li_{20}Si_6)^{4-}$			Acceptor $(Li_{22}Si_4)^{4+}$			Interaction active at the cluster units A, A', D, D'
	Atom	Site set	AO's	Atom	Site set	AO's	
I	Si	OH	$3p_z$	Li	OH	$2p_z$	(D, A'), (A, D')
II	Si	OH	$3p_x$	Li	CO	2 s/2 p	(D', A'), (D, A)
III	Li	CO	2 s/2 p	Si	OT	$3p_x/3p_y$	(D', A')

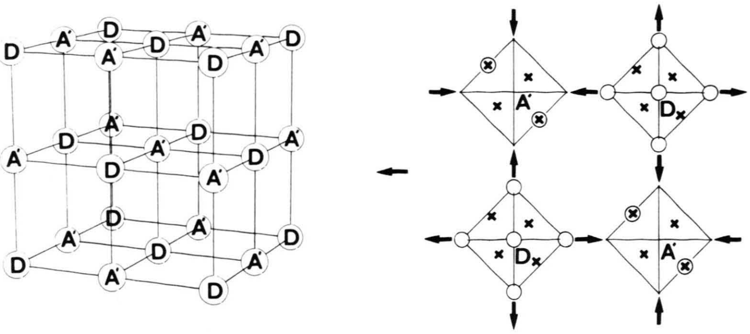

Fig. 12. Mutual coupling between those donor and acceptor centers that form the NaCl (sub)structures. *Right side:* The OH, OT and IT site sets of four neighbouring clusters at $z = 0$ are shown. The employed symbols are identical with the labels introduced in Figure 11. Donor-acceptor interactions are indicated by arrows. *Left side:* NaCl substructure formed by clusters at $z = 0$ and $z = 1/2$. An equivalent substructure is formed by the cluster units at $z = 1/4$ and $z = 3/4$ (see Figure 11).

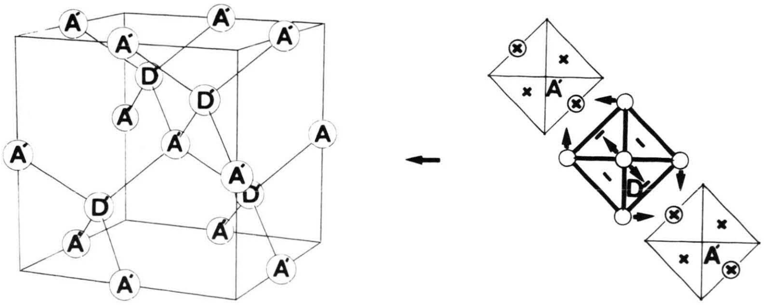

Fig. 13. Mutual coupling between donor and acceptor clusters leading to the ZnS substructures. *Right side:* The OH, OT and IT site sets of both units are shown as in Figure 11. Intercluster interactions (II) are indicated by arrows. They represent an electron transfer from the Si 3 p_x AO's of the donor unit (D, D′) to the Li functions of the CO site set of the acceptor units (A, A′), *Left side:* Simplified scheme of one of the resulting ZnS arrangements.

we have mentioned that this orientation has been explained by Pearson and coworkers on the basis of structural data [35]. The coupling mechanism I is an electronic rationalization of this behavior. In the last row of Table 13 we have collected those cluster species where this interaction is active. The two NaCl substructures can be identified without difficulties in Figure 11.

b) *Interaction-type II* leads to a coupling between the two NaCl substructures. Each reference cluster is surrounded by six nearest neighbors of his own substructure and eight cluster units that belong to the second substructure. The latter arrangement contains four donor and four acceptor species. The interaction II is determined by the coupling of one donor (acceptor) cluster to four neighboring acceptor (donor) units of the second NaCl substructure. This coupling allows for a charge transfer from the Si $3p_x$ AO's of the donor units to suitable Li functions of the CO site set in the acceptor. The spatial localization of the Si $3p_x$ AO's of D and D′ coincides with the internuclear axes of the OT atoms of the acceptor cluster. Figure 11 shows that this coupling is operative for all donor-acceptor contacts of the crystal structure. The connecting line between the OT site set of D and D′ points always into the direction of the A and A′ units. But this requires a 90° rotation of D′ relative to the orientation of A, A′ and D, respectively. This allows for the localization of the Si $3p_x$ functions of D′ into the direction of the acceptor unit A′. The interaction-type II corresponds to the formation of a ZnS structure type (Figure 13). The combined intercluster mechanism I and II; (formation of NaCl as well as ZnS substructures) leads to an cluster arrangement in $Li_{21}Si_5$ that corresponds completely with the classical Zintl-phase NaTl [5]: The two donor clusters $D, D' = (Li_{20}Si_6)^{4-}$ replace the Tl atoms, the acceptors $A, A' = (Li_{22}Si_4)^{4+}$ the Na atoms.

c) *Interaction-type III* corresponds to a charge transfer from the metal atoms of CO in the donor unit to the Si $3p_x/3p_y$ AO's of the acceptor. This coordination between the Si sites (D or D′) and the Li atoms (A and A′) is only observed for A′ D′ pairs (Figure 11). The coupling between the A and D units is not possible because the Si atoms of A′ (OT site set) are directed to A instead of D. The electronic origin for this behavior is simple to explain. A 90° rotation of A (in analogy to the

geometric modification of D′) renders possible such contacts, but is also accompanied by the creation of weak antibonding Si–Si contacts between the A and A′ clusters.

The analysis of the electronic structure of the $(Li_{22}Si_4)^{4+}$ acceptor clusters has shown that the Si atoms possess highly filled $3p_z$ AO's. This occupation can be understood in terms of a "back-transfer" of electrons from the acceptor (i.e. tetrahedral Si positions). The crystal structure contains remarkable Li–Si contacts in these regions. In the case of A′ this coupling is facilitated by an extension of the inner Li tetrahedron allowing for Li–Si bonds with cluster A. An analog interaction between D′ and A′ is possible by the 90° rotation of the donor component (Fig. 11 and Section 2).

8. Conclusion

The electronic structure of crystalline $Li_{21}Si_5$ has been investigated by a finite cluster approach in the framework of a semiempirical MO model of the INDO-type. The three-dimensional structure has been fragmented into formal donor and acceptor cluster units M_{26}. The composition and net charge of the unperturbed donor units D and D′ is $(Li_{20}Si_6)^{4-}$ while the acceptor fragments A and A′ are formed by $(Li_{22}Si_4)^{4+}$ clusters. The Li–Si interaction is mainly covalent and therefore determined by the kinetic energy of the valence electrons. The Li–Li contacts are nonbonding, at least in the framework of the mean-field approximation. The localization of the canonical MO's leads to a representation of the one-particle levels that render possible a straightforward interpretation of the electronic interactions in the cluster units. The transformed occupied MO's in $(Li_{20}Si_6)^{4-}$ are largely determined by the Si atoms. The various "Li–Si bonds" are of a nonclassical multi-center type that spans several Li sites in the direct neighborhood of the Si reference atom. This MO type conserves nevertheless the validity of the classical valence rules, e.g. the formation of Si^{4-} octets. In $(Li_{22}Si_4)^{4-}$ sixteen occupied orbitals are present, which are similar to the filled Si localized MO's of the donor, but in addition a seventeenth MO is formed, namely a delocalized cage orbital which is extended over the 2s AO's of the electropositive Li atoms. This function is completely independent of the former MO set, but preserves the extended octet configuration of the Si atoms. The complete 3 D crystal structure of $Li_{21}Si_5$ can be rationalized on the basis of the results derived for the clusters units $(Li_{20}Si_6)^{4-}$ and $(Li_{22}Si_4)^{4+}$. Three types of intercluster interactions have to be distinguished. Type I arranges the donor and acceptor cluster to a NaCl substructure. Type II cause additionally a ZnS arragement of both cluster units leading to the interpenetration of two NaCl substructures, typical for the NaTl structure type. A charge transfer from the cube-octahedral Li sites in the donor to Si atoms of the acceptor is the third type (III) of interactions that contribute to the intercluster coupling stabilizing the 3D structure of $Li_{21}Si_5$.

Acknowledgement

One of the authors (M.C.B.) has been supported by the Stiftung Volkswagenwerk.

[1] H. Schäfer, B. Eisenmann, and W. Müller, Angew. Chem. **85,** 742 (1973); Angew. Chem. Int. Ed. Engl. **12,** 649 (1973).
[2] H. G. von Schnering, Angew. Chem. **93,** 44 (1981); Angew. Chem. Int. Ed. Engl. **20,** 33 (1983).
[3] H. Schäfer and B. Eisenmann, Rev. Inorg. Chem. **3,** 29 (1981).
[4] E. Zintl and W. Dullenkopf, Z. Phys. Chem. **B 16,** 195 (1932); E. Zintl and G. Brauer, Z. Phys. Chem. **B 20,** 245 (1933).
[5] E. Zintl, Angew. Chem. **52,** 1 (1939).
[6] E. Mooser and W. B. Pearson, Phys. Rev. **101,** 1608 (1959).
[7] W. Klemm and E. Busmann, Z. Anorg. Allg. Chem. **319,** 297 (1963).
[8] W. Klemm, Proc. Chem. Soc. London **1958,** 329.
[9] A. Zunger, Phys. Rev. **B 17,** 2582 (1978).
[10] T. Asada, T. Jarlborg, and A. J. Freeman, Phys. Rev. **B 24,** 510 (1981).
[11] J. Robertson, Solid State Commun. **47,** 899 (1983).
[12] P. C. Schmidt, Phys. Rev. **B 31,** 5015 (1985).
[13] P. C. Schmidt, Z. Naturforsch. **40a,** 335 (1985).
[14] N. E. Christensen, Phys. Rev. **B 32,** 207 (1985).
[15] M. C. Böhm, R. Ramírez, R. Nesper, and H. G. von Schnering, Phys. Rev. **B 30,** 4870 (1984).
[16] M. C. Böhm, R. Ramírez, R. Nesper, and H. G. von Schnering, Ber. Bunsenges. Phys. Chem. **89,** 465 (1985).
[17] R. Ramírez, R. Nesper, H. G. von Schnering, and M. C. Böhm, Chem. Phys. **95,** 17 (1985).
[18] M. C. Böhm, Theor. Chim. Acta **62,** 351 (1983).
[19] M. C. Böhm and R. Gleiter, Theor. Chim. Acta **59,** 127, 153 (1981).

[20] H. Axel, H. Schäfer, and A. Weiss, Z. Naturforsch. **21b,** 115 (1966).
[21] R. Nesper, J. Curda, and H. G. von Schnering, manuscript in preparation.
[22] W. Hume-Rothery, J. Inst. Met. **35,** 307 (1926).
[23] W. Hume-Rothery, R. E. Smallman, and C. W. Haworth, The Structure of Metals and Alloys, 5th Ed., Institute of Metals, London 1969.
[24] T. Clark and P. v. R. Schleyer, J. Amer. Chem. Soc. **101,** 7748 (1979); E. D. Jemmis, J. Chandrasekhar, and P. v. R. Schleyer, J. Amer. Chem. Soc. **101,** 2848 (1979).
[25] A. J. Kos, D. Poppinger, and P. v. R. Schleyer, Tetrahedron Lett. 2151 (1980); Y. Apeloig, T. Clark, A. J. Kos, E. D. Jemmis, and P. v. R. Schleyer, Isr. J. Chem. **20,** 43 (1980).
[26] G. Graham, S. Richtmeier, and D. A. Dixon, J. Amer. Chem. Soc. **102,** 5759 (1980).
[27] E. D. Jemmis, J. Chandrasekhar, E.-U. Würthwein, P. v. R. Schleyer, J. W. Chinn, Jr., and F. J. Pople, J. Amer. Chem. Soc. **104,** 4275 (1982).
[28] P. v. R. Schleyer, E.-U. Würthwein, E. Kaufmann, T. Clark, and J. A. Pople, J. Amer. Chem. Soc. **105,** 5930 (1983).
[29] K. Krogh-Jespersen, J. Amer. Chem. Soc. **107,** 537 (1985).
[30] A. E. Reed and F. Weinhold, J. Amer. Chem. Soc. **107,** 1919 (1985).
[31] H. Bärnighausen, Match, Comm. Math. Chem. **9,** 139 (1980)
[32] H. G. von Schnering, R. Nesper, J. Curda, and K.-F. Tebbe, Angew. Chem. **92,** 1070 (1980); Angew. Chem. Int. Ed. Engl. **19,** 1033 (1980).
[33] R. Nesper, H. G. von Schnering, and J. Curda, J. Solid State Chem. **62,** 199 (1986).
[34] O. V. Heidenstam, A. Johansson, and S. Westman, Acta Chem. Scand. **22,** 653 (1968).
[35] M. H. Booth, J. K. Brandon, R. Y. Brizard, C. Chieh, and W. B. Pearson, Acta Cryst. **B 33,** 30 (1977); J. K. Brandon, R. Y. Brizard, W. B. Pearson, and D. J. N. Tozer, Acta Cryst. **B 33,** 527 (1977).
[36] M. C. Böhm, Inorg. Chim. Acta **62,** 171 (1982).
[37] J. A. Pople and D. L. Beveridge, Approximate Molecular Orbital Theory, McGraw Hill, New York 1970.
[38] D. R. Hartree, The Calculation of Atomic Structure, Wiley Interscience, New York 1957.
[39] R. S. Mulliken, J. Chem. Phys. **23,** 1833 (1955).
[40] K. B. Wiberg, Tetrahedron **24,** 1083 (1968).
[41] C. Edmiston and K. Ruedenberg, Rev. Mod. Phys. **35,** 457 (1963); C. Edmiston and K. Ruedenberg, J. Chem. Phys. **43,** 597 (1965).
[42] W. Kutzelnigg, Angew. Chem. **96,** 262 (1984) and references cited herein; Angew. Chem. Int. Ed. Engl. **23,** 272 (1984).
[43] R. McWeeny and B. T. Sutcliffe, Methods in Molecular Quantum Mechanics. Academic Press, New York 1969.
[44] G. D. Graham, D. S. Marynick, and W. N. Lipscomb, J. Amer. Chem. Soc. **102,** 4572 (1980).
[45] K. D. Sen, M. C. Böhm, and P. C. Schmidt, J. Molec. Struct. (Theochem) **106,** 271 (1984).
[46] E.-U. Würthwein, P. v. R. Schleyer, and J. A. Pople, J. Amer. Chem. Soc. **106,** 6973 (1984); P. v. R. Schleyer, B. Tidor, E. D. Jemmis, J. Chandrasekhar, E.-U. Würthwein, A. J. Kos, B. T. Luke, and J. A. Pople, J. Amer. Chem. Soc. **105,** 484 (1983).
[47] M. C. Böhm and P. C. Schmidt, Ber. Bunsenges. Phys. Chem., in press.
[48] L. Salem, J. Amer. Chem. Soc. **90,** 543 (1968); L. Salem, Chem. Brit. **5,** 449 (1969).